sustainability

MDPI

Article

How Do the Dynamics of Urbanization Affect the Thermal Environment? A Case from an Urban Agglomeration in Lower Gangetic Plain (India)

Arijit Das [1], Priyakshi Saha [1], Rajarshi Dasgupta [2], Miguel Inacio [3], Manob Das [1,*] and Paulo Pereira [3]

[1] Department of Geography, University of Gour Banga, Malda 732103, India; arijit3333@gmail.com (A.D.); priyakshisaha63@gmail.com (P.S.)
[2] School of Public Policy, IIT Delhi, Hauz Khas, New Delhi 110016, India; rajarshidg1@yahoo.co.in
[3] Environmental Management Laboratory, Mykolas Romeris University, Atheties St. 20, LT-08303 Vilnius, Lithuania; rinacio.miguel@gmail.com (M.I.); pereiraub@gmail.com (P.P.)
* Correspondence: dasmanob631@gmail.com

Abstract: Urban growth and development has significantly affected urban heat island (UHI) due to urbanization. Particularly in the cities in developing countries, the assessment of UHI has emerged as one of the core research themes as it significantly affects the ecological environment and livability in cities. Thus, the assessment of UHI is crucial for climate mitigation and sustainable urban landscape planning. This study identifies the dynamics of landscape patterns and the impact of composition and configuration on the thermal environment in English Bazar Urban Agglomeration (EBUA), Eastern India, along the urban–rural gradient (URG) approach. Geospatial approaches and spatial metrics were employed to assess the impact of the landscape pattern on the thermal environment. Descriptive and inferential statistics have also been used to find the effects of landscape patterns on the thermal environment. The result has also been validated based on the location and correlation analysis. The built-up area increased by about 63.54%; vegetation covers and water bodies declined by 56.72% and 67.99% from 2001 to 2021. Land surface temperature (LST) decreased with increasing distance from the core of the city. LST declined by about 0.45 °C per kilometer from the core of the city towards the outside. LST had a positive correlation with IS and a negative correlation with green space (GS) and blue space (BS). The mean aggregation of the impervious patches was larger (73.21%) than the GS (43.18%) and BS (49.02%). The aggregation of impervious surface (IS) was positively correlated, and aggregations of GS and BS had a negative correlation with LST. Findings suggest that the spatial composition and configuration of the impervious surface, GS, and BS must be considered in landscape planning and design framework to make the city more livable.

Keywords: urban heat island; urban agglomeration; GS; landscape pattern; landscape planning

check for updates

Citation: Das, A.; Saha, P.; Dasgupta, R.; Inacio, M.; Das, M.; Pereira, P. How Do the Dynamics of Urbanization Affect the Thermal Environment? A Case from an Urban Agglomeration in Lower Gangetic Plain (India). *Sustainability* **2024**, *16*, 1147. https://doi.org/10.3390/su16031147

Academic Editor: Baojie He

Received: 30 December 2023
Revised: 20 January 2024
Accepted: 22 January 2024
Published: 30 January 2024

Copyright: © 2024 by the authors. Licensee MDPI, Basel, Switzerland. This article is an open access article distributed under the terms and conditions of the Creative Commons Attribution (CC BY) license (https://creativecommons.org/licenses/by/4.0/).

1. Introduction

Urbanization is one of the significant anthropogenic impacts on the earth in terms of land use and land cover (LULC) [1,2]. Thus, urbanization has a crucial impact on the thermal environment and the emergence of the urban heat island (UHI) effect [3,4]. Urbanization transforms the natural land cover into artificial surfaces [5]. The impacts of anthropogenic activities are more prominent due to unplanned urbanization [6,7]. Thus, the LULC dynamics largely affect urban and sub-urban landscapes, leading to the increase in temperature and the emergence of the UHI effect [8,9]. The temperature in the urban areas is higher than the surrounding environment [10,11]. The emergence of the UHI effect significantly affects people's quality of life and results in eco-environmental degradation [12]. Besides ecological consequences, the UHI effect also causes deterioration of air quality, human health, and thermal comfort level [13,14]. Therefore, the assessment and monitoring of UHI has become one of the significant research issues in urban climatology,

urban landscape, and urban geography [15,16]. The changes in surface properties are the prime factors affecting the UHI effect [15]. Therefore, it is crucial to explore the relationship between landscape patterns, composition, configuration, and the urban thermal environment (UTE) [2,17,18]. These studies showed that landscape patterns had a tremendous impact on LST. Maimaitiyiming et al. [19] conducted a survey in Asku city in China and showed the impact of green space (GS) on the land surface temperature (LST). According to Asgarian et al. [20], the connectivity and complexity of the urban landscapes increased LST due to the high energy between landscapes. The loss of GS and blue space (BS)increased LST, whereas the expansion of GS generates a cooling effect in urban areas [21]. However, most studies were conducted on the relationship between LST and land cover types [22,23]. The impact of landscape configuration and composition on the LST from the perspective of UHI is essential for climate-sensitive planning strategies in cities [5].

Globally, accelerated urbanization, continued population growth, and loss of green infrastructures (GI) increased temperatures, significantly affecting human health and thermal comfort level [7,24]. At the Climate Conference (2018) in Paris, it was stated that the temperature across the globe increased substantially, and several recommendations were suggested, such as reducing carbon emissions and green house gas (GHG) and use of renewable energy [24]. Thus, studying and understanding the UHI phenomenon is crucial to reducing the influence of climate change and finding possible measures and strategies [7]. UHI effect can be accessed from two perspectives, namely UHI related to the surface (SUHI) and UHI related to the atmosphere (AUHI) [25]. SUHI is assessed based on the LST, and AUHI is assessed based on the air temperature [7]. This study analyzed UHI based on the LST retrieved from remote sensing (RS). The rapid urban expansion and population growth in the cities of developing countries have strengthened the UHI effect [26]. In India, very limited studies were carried out on the relationship of landscape composition with LST from the perspectives of UHI phenomena. English Bazar Urban Agglomeration (EBUA) has extended because of the growth of the population and rapid urban expansion [27]. Recent studies showed that EBUA had experienced a dramatic transformation of LULC and a significant increase in built-up areas [27,28]. For example, according to Dutta and Das [29], the EBUA built area increased from 6.99% (14.75 KM^2) to 7.22% (15.80 KM^2). Dutta and Das [29] conducted another study in EBUA on the spatiotemporal pattern of regional heat islands (RHI) and found that mean LST increased by 1.73 °C from 1990 to 2015. A study performed by Ziaul and Pal [30] to examine the outdoor thermal comfort (OTC) level in EBUA found that the area under highly uncomfortable areas increased from 3281.4 ha (2010) to 4815 ha (2016). Thus, from the previous research studies, a few notable research gaps can be highlighted. Firstly, previous studies mostly focused on the identification of urban growth patterns, landscape fragmentation due to urban expansion, the pattern of UHI, and the relationship between LULC and LST. However, the impact of urbanization on the thermal environment with a validated framework has remained unexplored. This is the first attempt to explore the impact of urbanization on the thermal environment with a validated framework. This study aims to explore the influence of landscape pattern, composition, and configuration on the thermal environment using geospatial and gradient approaches. The fundamental objective of this study is to explore the impact of landscape pattern, composition, and configuration on thermal environment along URG.

2. Materials and Methods

2.1. Study Area

EBUA is located in Eastern India, and it is the sixth largest urban agglomeration in West Bengal (WB), with an area of 5465.43 ha comprising both urban centers (English Bazar Municipality and Old Malda Municipality), census towns (such as Baghbari, Chatian more), and surrounding rural areas (Figure 1 and Table 1). EBUA has a population density of 13,861 persons/km^2. From 1991 to 2001 and 2001 to 2011, the decadal growth of the population was 24.78% and 21.50% [28]. EBUA is located on the Western bank of the Mahanada river and flows in the middle portion of EBUA (which divides English Bazar

Municipality from Old Malda Municipality). The annual mean temperature is about 25.4 °C, with temperatures ranging from 21 °C in winter (December and January) to 46 °C in summer (May and June).

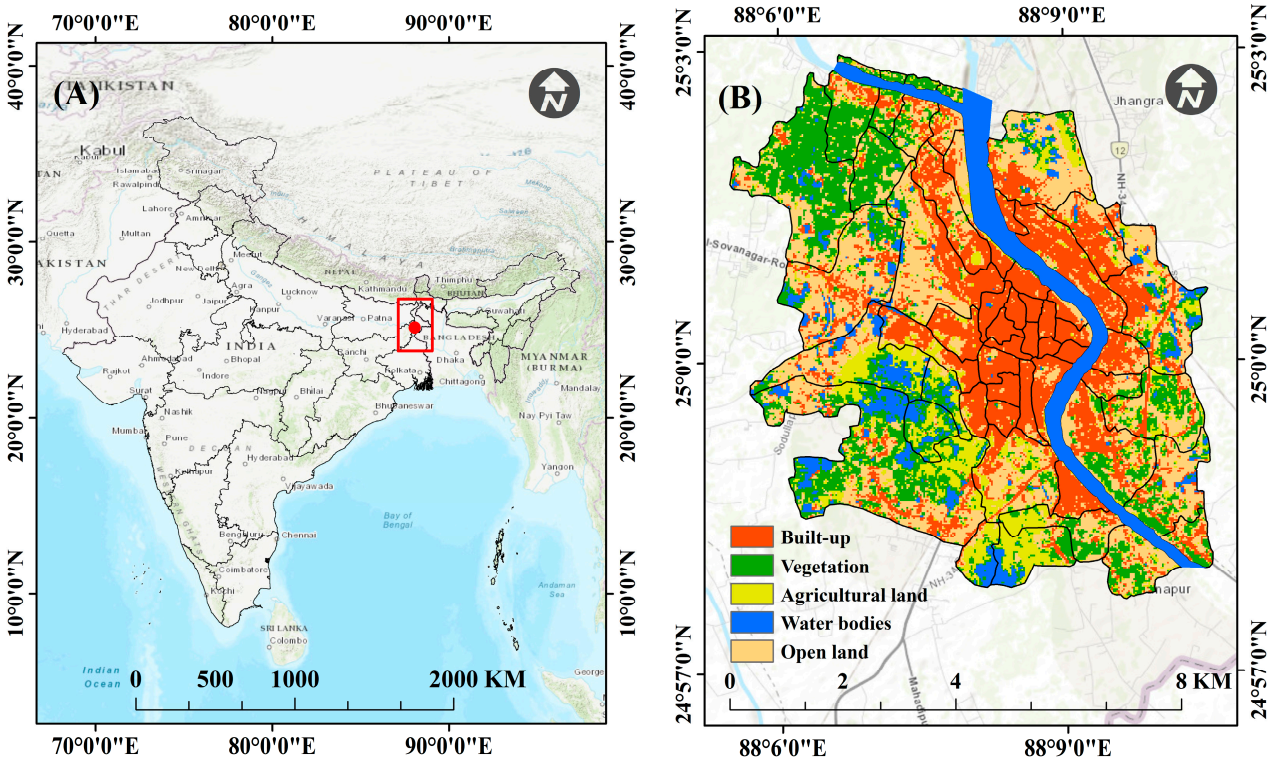


Figure 1. Location map of the research area. (**A**) Location of EBUA in India. (**B**) LULC map of EBUA (2021).

Table 1. Profile of EBUA.

Basic Information	
Name	English Bazar Urban Agglomeration (EBUA)
City type	Class I city (sixth largest urban agglomerations in West Bengal)
Local bodies	(i) Municipalities (English Bazar and Old Malda), (ii) Census towns, (iii) Mouzas (16 from English Bazar block and 11 from Old Malda block)
Urban bodies	2 municipalities,
Area (km^2)	5465.43 ha [28]
Geographical location	Diara region in lower Gangetic plain
Demographic profile	
Total population	0.63 million
Population density (person/km^2)	13,861
Decadal growth (%)	21.5
Climatic features	
Climate type	Sub-tropical monsoon
Season	(i) Monsoon–June to mid of October; (ii) Post-monsoon–mid of October to mid of December; (iii) Winter–January to February, and (iv) Pre-monsoon (Summer)–March to May
Temperature (°C) in winter	About 10
Temperature (°C) in summer	About 35
Precipitation (mm)	1444

2.2. Data Source

Landsat 5 Thematic Mapper (TM) and Landsat 8 Operational Land Imager (OLI) sensors with a 30 m spatial resolution have been used as remotely sensed satellite images

(Table 2). The Landsat 5 TM was captured on 14 April 2001 and 25 April 2011, and Landsat 8 OLI images were captured on 15 March 2021, with path and row 139 and row 43. All the satellite images were downloaded from the United States Geological Survey (USGS) online portal. Landsat TM and Landsat OLI have been used to develop LULC maps and retrieve LST. In the case of TM, it consists of seven multi-spectral bands; among them, Band 6 is considered a thermal band. On the other hand, Landsat OLI consists of eleven Bands, and Bands 10 and 11 are thermal bands. Thus, Band 6 (for Landsat TM) and Band 10 (for Landsat OLI) have been used as thermal bands to extract LST for the years 2001, 2011, and 2021.

Table 2. Datasets used.

Year	Specification of Date	Image ID	Resolution (Meter)	Sensor
2001	25 April	LT05_L2SP_139043_20010425_20200906_02_T1	30	Thematic mapper (TM)
2011	4 April	LT05_L2SP_139043_20110421_20200822_02_T1	30	Thematic mapper (TM)
2021	15 March	LC08_L2SP_139043_20210315_20210328_02_T1	30 (100 m for thermal band)	Operational Landsat imager

2.3. LST Extraction

Landsat 5 TM (Band 6) and Landsat 8 OLI (Band 10) have been used to produce LST maps for the years 2001, 2011, and 2021, comprising the top of the atmospheric brightness temperature values in Kelvin. There are three basic algorithms to retrieve LST: transmittances, emissivity, and, thirdly, means of atmospheric temperature, respectively. At first, the DN (digital number) values were converted into absolute radiance values using the following equation:

$$L_\lambda = M_L \cdot Q_{cal} + A_L \quad (1)$$

where L_λ refers to TOA spectral radiance (Watts/($m^2 \times sr \times \mu r$)); Q_{cal} refers to the DN values of thermal bands; A_L means additive re-scaling factor (band-specific); and M_L is multiplicative re-scaling factor (band-specific).

The at-satellite brightness temperature (T_β) has been calculated from spectral radiance (L_λ) and calibration constant (K1, K2). According to the nature of the landscape, the spectral emissivity correction is calculated:

$$T_\beta = \frac{\boldsymbol{K2}}{\boldsymbol{In}(\frac{\boldsymbol{K1}}{\boldsymbol{L\lambda}} + \mathbf{1})} \quad (2)$$

Basically, TOA is revealed in the Kelvin (K) unit, which was later transformed to degrees Celsius (°C). The following equation is used for calculating the emissivity-corrected LST.

$$LST = \frac{\boldsymbol{T\beta}}{\mathbf{1} + \left(\boldsymbol{\lambda} * \frac{\boldsymbol{T\beta}}{p}\right)\boldsymbol{In\varepsilon}} \quad (3)$$

where λ refers to the center wavelength of the emitted transmittance; $p = h \times c/k$ (1.438×10^{-2} m k); h = Planks constant (6.626×10^{-34} Js); k = Boltzmann constant (1.38×10^{-23} Js); c = velocity of light; and $\boldsymbol{\varepsilon}$ is the land surface emissivity.

$$\varepsilon = mp_{fc} + n \quad (4)$$

where

$$m = (\varepsilon_V - \varepsilon_Y) - (1 - \varepsilon_x)\, F\varepsilon_X \text{ and,}$$

$$n = \varepsilon_x + (1 - \varepsilon_x)F\varepsilon,$$

ε_v and ε_s refers to the vegetation and soil emissivity; F is the shape factor (mean value is 0.55); and p_{fc} is the vegetation proportion.

$$p_{fc} = \left(\frac{\boldsymbol{NDVI} - \boldsymbol{NDVI_{MIN}}}{\boldsymbol{NDVI_{MAX}} - \boldsymbol{NDVI_{MIN}}}\right)^2 \quad (5)$$

NDVI refers to the normalized difference vegetation index retrieved by using Equation (5).

2.4. LULC Mapping and Extraction of the IS, GS and BS

The spectral index-based method has been used to develop LULC maps in EBUA for 2001, 2011, and 2021. The satellite images have been classified into five classes: built-up areas, vegetation cover, agricultural land, water bodies, and open or bare land. The IS were extracted using the normalized difference built-up index (NDBI). GS were extracted from the normalized difference vegetation index (NDVI), and the normalized difference water index (NDWI) was used to extract BS.

$$\boldsymbol{NDBI} = \frac{\boldsymbol{MIR} - \boldsymbol{NIR}}{\boldsymbol{MIR} + \boldsymbol{NIR}} \quad (6)$$

where NIR refers to Band 4 and Band 5 (for Landsat TM and OLI), whereas MIR refers to Band 5 and Band 6 (for Landsat TM and OLI) [31,32].

$$\boldsymbol{NDVI} = \frac{\boldsymbol{NIR} - \boldsymbol{RED}}{\boldsymbol{NIR} + \boldsymbol{RED}} \quad (7)$$

where NIR refers to Band 4 and Band 5 (for Landsat TM and OLI), and RED refers to Band 3 and Band 4 (for Landsat TM and OLI) [32].

NDVI has been applied to extract GS. Usually, it is calculated for plant coverage and growth monitoring in a study area.

$$\boldsymbol{NDWI} = \frac{\boldsymbol{NIR} - \boldsymbol{MIR}}{\boldsymbol{NIR} + \boldsymbol{MIR}} \quad (8)$$

where NIR refers to Band 4 and Band 5 (for Landsat TM and OLI), and MIR refers to Band 5 and Band 6 (for Landsat TM and OLI) [33].

In this study, the percentage of GS and BS has been calculated to show the relationship between GS and BS with LST. GS refers to the percentage of GS in each buffer, and BS refers to the percentage of BS in each buffer. Thus, GS/BS refers to the sum of all the GS and BS concerning to the total areas in the buffer.

2.5. Delineation of UHI

The land surface temperature variation index (LSTVI) was computed to analyze the outcome of UHI. The LSTVI explores the effectiveness of UHI quantitatively, and as a result, a UHI intensity image is produced. LSTVI can be used as one of the significant indices to find out the effectiveness of the UHI phenomenon in any area based on the LST. The following equation has been used to calculate LSTVI:

$$\text{LSTVI} = \left(\frac{\boldsymbol{ST}_p - \boldsymbol{T_{mean}}}{\boldsymbol{T_{mean}}}\right) \quad (9)$$

where ST_p refers to the LST of a particular point, and T_{mean} refers to the mean LST of the entire study landscape.

2.6. Spatial and Statistical Analysis

2.6.1. Multi-Ring Approach

URG analysis has typically been carried out to observe the spatial variation of LST and the impact of IS, GS, and BS on LST. URG has been analyzed using a multi-ring buffer (MRB) approach to find the impervious surface, GS, and BS distribution over each buffer zone. MRB zones have been developed from the city's core with an interval of 300 m up to

4500 m for three years (2001, 2011, and 2021). LST, impervious surface, GS, and BS have been obtained from each buffer zone, and a correlation analysis has been conducted. URG analysis provides significant findings to understand the spatial variations and distribution among various parameters in the study landscape. A bi-variate Spearman correlation analysis was carried out to show the relationship of LST with IS, GS, and BS.

2.6.2. Spatial Metrics-Based Analysis

The study area has been divided into 20 buffers from the city center with an interval of 300 m. Each buffer was clipped from the LULC map. Thus, the extracted LULC map was utilized as input in this analysis. Lastly, three class-level spatial metrics (area mean, shape mean, and aggregation index) were selected to represent the size, aggregation, shape, and complexity (Table 3). The area of landscapes influences the thermal patterns in cities. The areas with higher built-up regions are characterized by higher temperatures [32]. The GS and BS have significant cooling effects and decrease temperature [32]. The mean shape area of the landscapes changes thermal patterns. The higher mean shape area of IS reveals higher LST. The aggregation of GS and BS decreases the temperature. The temperature from the city towards the fringe decreases due to a higher aggregation of GS and BS than IS. Thus, understanding the impact of area, shape area, and aggregation of the landscapes is crucial for thermal pattern analysis in cities. All these analyses were performed using Fragstate (version 4.3) software [34]. The methodological framework of the entire research work is shown in Figure 2.

Table 3. Spatial metrics used.

Spatial Metrics	Acronym	Description
Mean patch area	AREA_MN	It is used to measure the area or size of the patch It is the sum of all patches of the corresponding path types. It is calculated from the patch metrics values divided by the number of patches. The equation of AREA_MN = $\frac{1}{1000\times n} \times \sum_{i=1}^{n} x_i$
Mean patch index	SHAPE_MN	It is one of the simplest measures of shape complexity It is calculated from the patch perimeter and square root of the patch areas, adjusted by a constant to adjust a square standard, and divided by the number of patches. The equation of SHAPE_MN = $\frac{1}{n} \times \frac{0.25\ P_l}{\sqrt{X_l}}$.
Aggregation index	AI	It is the number of like adjacencies divided by the maximum possible number of the adjacencies (corresponding class). The equation of AI = $\frac{g_i}{max-g_i} \times 100$ The value of AI "0" means totally disaggregated (no adjacencies), and 100 means patch type is totally aggregated, indicating a single patch.

A number of descriptive and inferential (correlation and regression) statistical analyses were carried out to understand the impact of the urban dynamics on the thermal environment. All the statistical analysis was carried out in SPSS (version 22).

2.6.3. Validation

In this research work, the impact of urbanization-induced LULC on the thermal environment has been verified using two methods: location-based methods and correlation-based methods. In the case of the location-based methods, the UHI maps were verified from Google Earth images in 2021 [35]. For correlation, the global human settlement layer (GHSL) has been used to find out the impact of impervious surfaces on the UHI. In previous studies, the IS has been used as one of the important indicators for urbanization, and it has a positive impact on the UHI in urban areas [36].

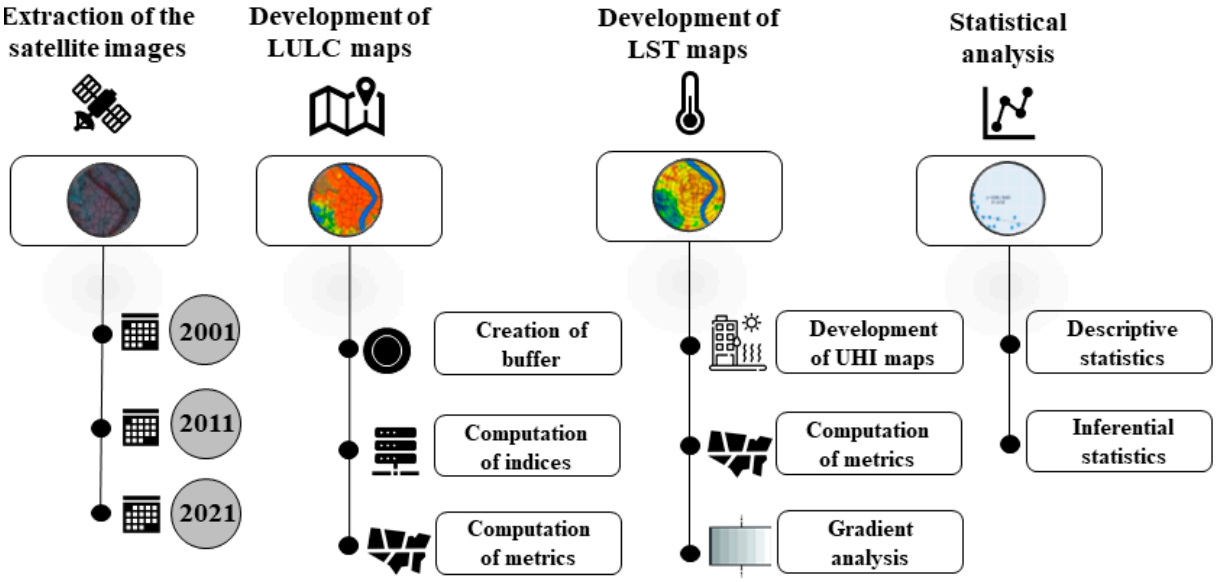


Figure 2. Methodological framework used.

3. Results

3.1. Validation

Location-based validation: Google Earth images were used (Supplementary Figure S1) to validate thermal patterns in EBUA based on the locations. The areas with higher GS and BS were characterized by lower LST and UHI, and built areas were characterized by higher LST and UHI intensity. For example, near the center of the city (at 300 m buffer), the average LST was 43.67 °C (with more than 99% of built-up aggregation), and outside of the city (at 4500 m buffer), the average LST was 41.35 °C (with aggregation of 44.86% built-up area).

Correlation-based validation: The validation of the results is presented in Figure 3. Overall, the model showed better performance, indicating that the built-up surface has a significant positive impact on the LST in EBUA (r = 0.86, $p > 0.001$) and explained 84% of the model. Thus, the study's findings are robust, and it is well accepted that IS has a significant impact on the thermal environment (e.g., LST).

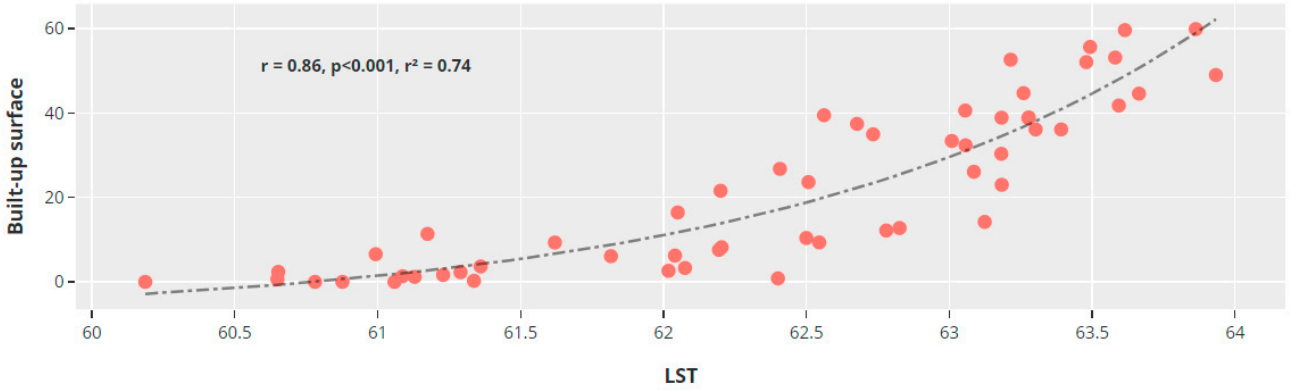


Figure 3. Regression between LST and built-up surface (GHSL). The dotted line shows the exponential line.

3.2. LST and UHI Pattern along URG

In 2001, the mean LST was 38.03 °C with a maximum and minimum of 39.64 °C and 27.64 °C. In 2011, the mean LST was 38.37 °C, with maximum and minimum LST of 39.36 °C and 27.56 °C. In 2021, the mean LST was 42.47 °C, with full and minimum LST

of 43.67 °C and 41.35 °C. Most of the middle parts of EBUA were characterized by very high LST. The northwestern, southwestern, and southeastern parts were characterized by relatively low LST (Supplementary Figure S2).

The LST decreases with increasing distance from the core. For example, in 2001, the mean LST at buffer 300 m was 39.64 °C, which declined to 38.35 °C at 2100 m buffer, 38.04 °C at 3000 m buffer, and 37.65 °C at 4200 m buffer. Thus, mean LST decreased by about 1.10% per kilometer (0.49 °C per kilometer) in 2001. In 2011, the mean LST was 38.94 °C at 300 m buffer, which reached 37.76 °C at 2100 m buffer, 37.64 °C at 3000 m, and 37.55 °C at 4200 m buffer. Thus, the mean LST decreased by about 0.45 °C (decreased by about 1.15%) per kilometer. In 2021, the mean LST decreased by 0.52% per kilometer from the core of the city towards the outside (Figure 4). Thus, the average decrease of LST was 0.45 °C (1.16%) per kilometer from the core during 2001 to 2021.

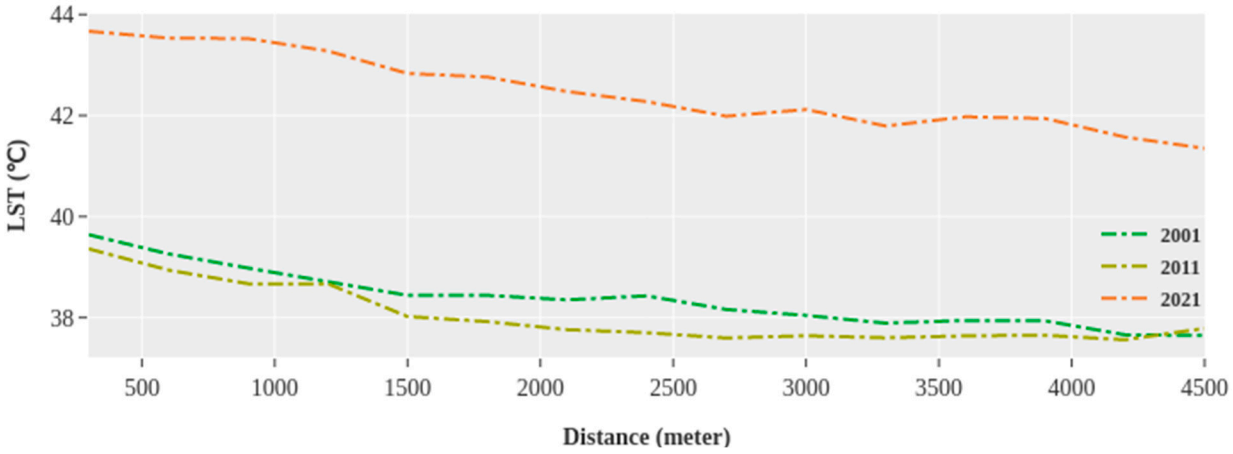


Figure 4. LST along the urban–rural gradient from 2001 to 2021.

Figure 5 elucidates the spatial and temporal variation of the LSTVI from 2001 to 2021. In 2001, 1.60% of the area came under very high LSTVI, which decreased to 0.60% in 2011 and increased to 1.53% in 2021. Similarly, in 2001, 16.75% of the area was covered with high LSTVI, which decreased to 3.75% in 2011 and increased to 27.02% in 2021. The areas with low LSTVI zones covered 10.58% in 2001, 5.61% in 2011, and 2.12% in 2021. The areas with low LSTVI zones increased from 23.92% to 34.11%.

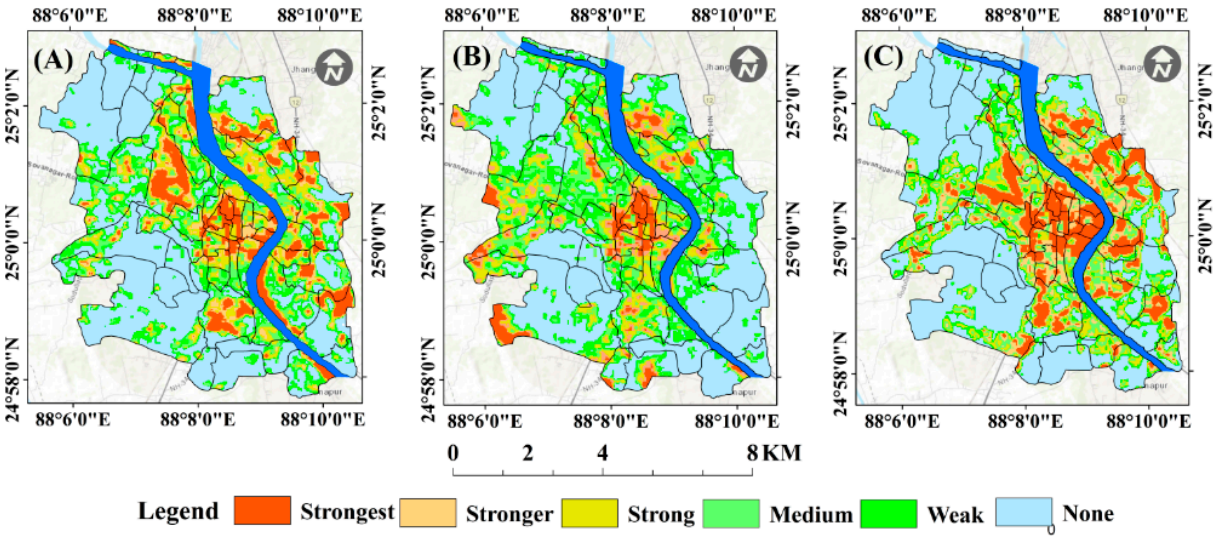


Figure 5. The spatial variation of UHI in EBUA (**A**) 2001, (**B**) 2011, and (**C**) 2021.

3.3. Changes of IS, GS, and BS along URG

The results showed that IS decreases and green and BS increase with increasing distance from the core. Buffers from 300 to 1500 m (1.5 km from the core) covered more than 40% of the total IS, and buffers from 3000 to 4500 m (1.5 km from up to the outer boundary) covered about 15% of the total IS from 2001 to 2021. GS at buffer 300 m was <1%, which increased to 10% at 4500 m buffer. The proportion of the BS was also deficient at the core (at buffer 300 m) that reached to 6% at buffer 4500 m (Figure 6).

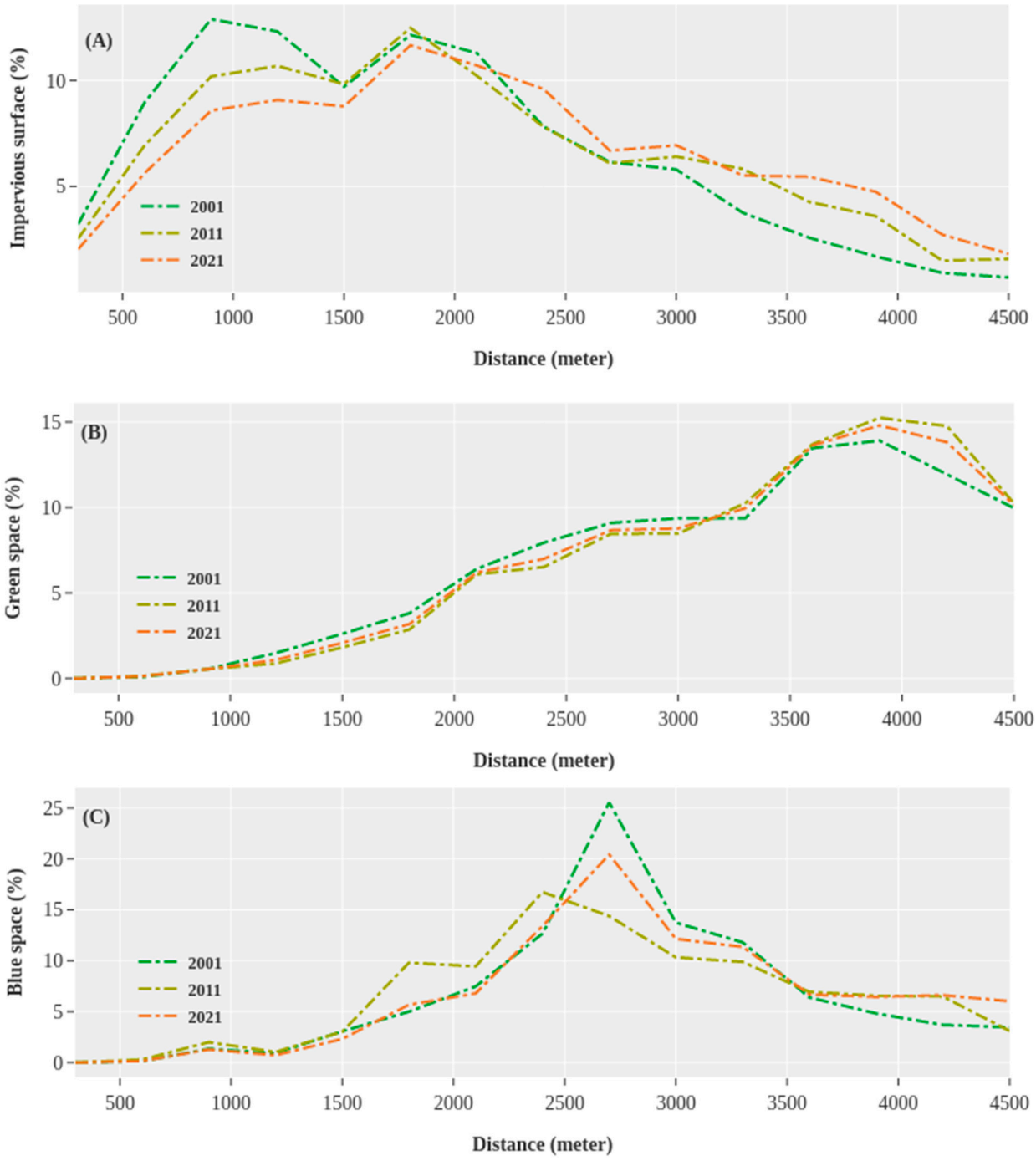


Figure 6. Changes of the (**A**) impervious surface, (**B**) GS, and (**C**) BS along the URG.

The results showed that LST was positively correlated with IS and negatively correlated with GS and BS (Figure 7). In 2001, the correlation between LST and IS was 0.715

(significant at 0.01), whereas the correlation was 0.412 in 2011 and 0.429 in 2021. The correlation between IS and GS was r = −0.943 (significant at 0.01) in 2021, followed by r = −0.938 in 2011 (significant at 0.01), and r = −0.870 in 2001 (significant at 0.01). The highest negative correlation between LST and BS was in 2021 (r = −0.828) (significant at 0.01), followed by in 2011 (r = −0.735) (significant at 0.01), and in 2001 (r = −0.536) (significant at 0.05).

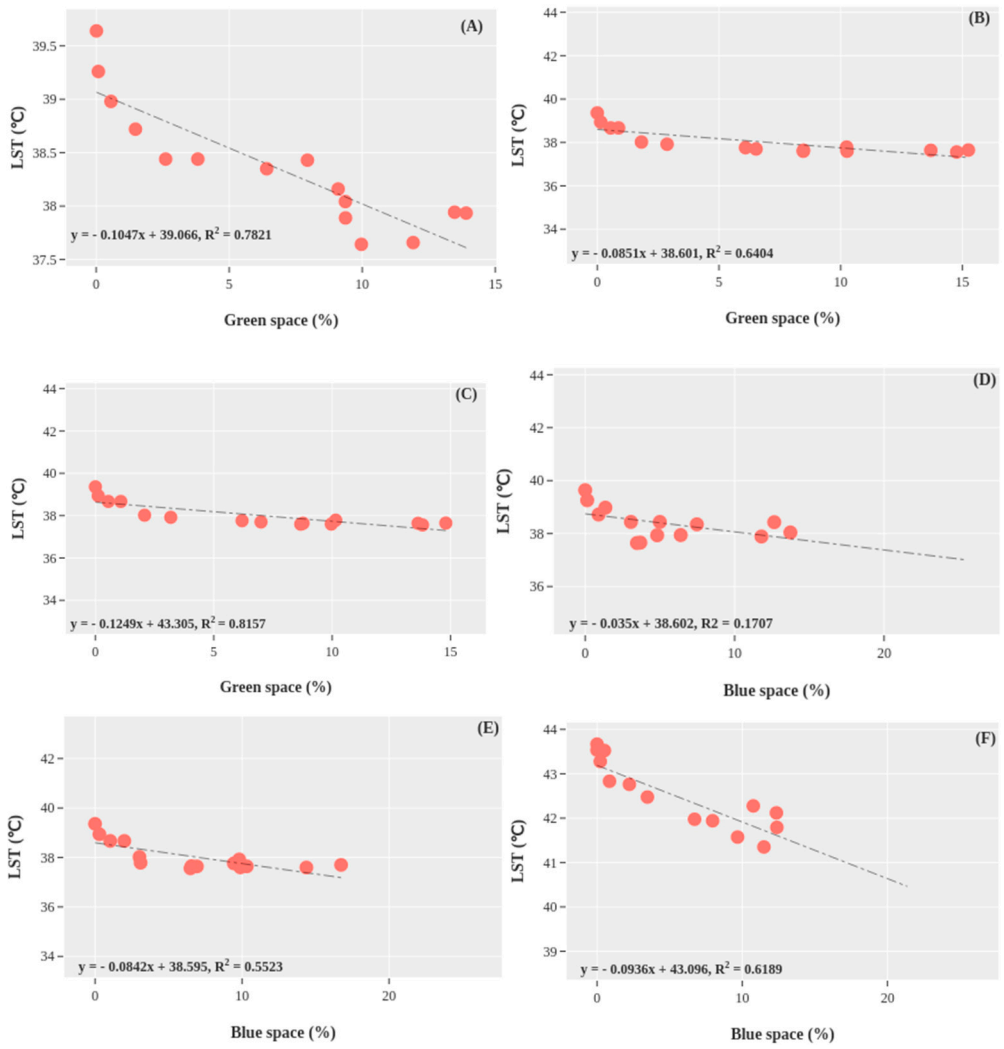


Figure 7. Relationship of LST with GS (**A**) 2001, (**B**) 2011, and (**C**) 2021 and BS (**D**) 2001, (**E**) 2011 and (**F**) 2021.

3.4. Impact of Landscape Composition and Configuration on the Thermal Environment

The spatial metrics across the buffer zones from the city center varied (Supplementary Figure S4). For example, in the case of IS, AREA_MN decreases with increasing distance from the core, and AREA_MN of GS and BS increases with increasing distance. AREA_MN of IS at 300 m buffer was 28.28 (ha) (GS = 0; BS = 0), which reached 0.380 (ha) (GS = 1.39; BS = 2.02) at 4500 m buffer. The average AREA_MN of all the buffer zones from the city to outside was 42.47 ha, whereas it was 0.769 ha for GS and 0.644 ha for BS. The SHAPE_MN of IS was 1.14 at 300 m buffer (GS = 0 and BS = 0). The average SHAPE_MN of IS for all the buffers was 1.85, whereas it was 1.20 for GS and 1.11 for BS. In the case of AI, IS decreases, and green and BS increase with distance from the core of the city. For example, AI at 300 m buffer zone was 99.22% (GS = 0%; BS = 0%), which declined to 44.86% (GS = 70%; BS = 82.01%) at 4500 m buffer zones.

Table 4 shows the correlation between spatial metrics and mean LST in EBUA, along with descriptive statistics. The highest AREA_MN was observed from IS (22.51 ha), followed by GS (0.77 ha) and BS (0.64 ha). The standard deviation (SD) was the highest for IS (40.12 ha), followed by green (0.55 ha) and BS (0.47 ha), indicating the greater variability of AREA-MN of IS than the green and BS. There was a strong positive correlation (r = 0.703) between AREA_MN (impervious surface) and LST, and LST had a strong negative correlation with GS (−0.896) and BS (r = −0.800). Thus, AREA_MN of the IS had a positive impact on the LST, and green and BS had a negative impact on the LST.

Table 4. Correlation between spatial metrics and mean LST (** indicates significates at <0.05).

Landscapes	Statistics	AREA_MN (ha)	SHAPE_MN (ha)	AI (%)
IS	Mean	22.51	1.86	73.22
	SD	40.12	1.23	17.64
	Skewness	2.09	1.61	−0.17
	Kurtosis	3.91	2.36	−1.26
Correlation with mean LST	r	0.703 **	0.217	0.960 **
	Sig (2-tailed)	0.003	0.437	0.000
GS	Mean	0.77	1.21	43.19
	SD	0.55	0.40	28.93
	Skewness	0.58	−1.64	−0.78
	Kurtosis	0.37	7.00	−1.19
Correlation with mean LST	r	−0.896 **	−0.363	−0.952 **
	Sig (2-tailed)	0.000	0.1784	0.00
BS	Mean	0.64	1.12	49.02
	SD	0.47	0.34	24.15
	Skewness	1.15	−1.99	−1.12
	Kurtosis	1.67	6.89	0.02
Correlation with mean LST	r	−0.800 **	−0.686 **	−0.722 **
	Sig (2-tailed)	0.000	0.005	0.002

The mean SHAPE_MN was the highest for IS (1.86 ha) followed by GS (1.21 ha) and BS (1.12 ha) space. The standard deviation (SD) was also highest for IS (1.23 ha), followed by green (0.40 ha) and BS (0.34 ha). The highest standard deviation (SD) for IS indicates the fact that there was a greater variability of SHAPE_MN than GS and BS. There was a very poor positive correlation between SHAPE_MN and LST (r= 0.217) and a poor negative correlation between GS and LST (r= −0.363). For BS, there was a strong positive correlation between SHAPE_MN and LST (r = −0.686).

The highest AI was observed from IS (73.22%) followed by BS (49.02%) and BS (43.19%). The standard deviation (SD) was the highest for GS (28.93%), followed by blue-green (24.15%) and IS (17.64%), indicating the greater variability of AI of the GS and BS than IS. There was a strong positive correlation between AI (impervious surface) and LST (r = 0.960), and LST had a strong negative correlation with GS (−0.952) and BS (r = −0.722). Thus, AI of the IS positively impacted the LST, and GS and BS negatively impacted the LST. The details of the relationship between LST and spatial metrics have been shown in the supplementary section (Supplementary Figure S5).

4. Discussion

The study's results showed that LST declined with increasing distance from the city due to a higher proportion of GS and BS. The GS and BS have the capacity to absorb the temperature through the process of photosynthesis and shading [32]. The AREA_MN at the 300 m buffer zone was 28.28 (ha), and LST was 43.67 °C, which reached 41.35 °C with AREA_MN of 0.380 (ha). The AREA_MN of GS was 1.39 ha (BS = 2.02 ha) at the buffer of 4500 m, with an average LST of 41.35 °C. It denotes that the IS had a more significant impact on the LST than the GS and BS. These findings suggest that significant coverage of GS and BS is crucial to mitigating the warming effect in cities [32,37]. The mean LST was about

2.32 °C higher in IS (in the city core) compared to the GS and BS. Sun et al. [38] conducted a study in Guangzhou in China and found a difference in mean LST (about 2.8 °C) between IS and GS. Song et al. [39] performed a study in Beijing (China) and reported a difference of 3.4 °C between GS and impervious. Estoque et al. [32] studied major cities of Southeast Asia and found a difference in mean LST between GS and IS (2.2 °C in Bangkok, 2.9 °C in Jakarta, and 3.7 °C in Manila). These findings revealed that GS and BS had a significant impact on the mitigation of the temperature (e.g., the UHI effect). Other studies also show the difference in mean LST between IS and GS (such as grassland, croplands, and pasture). For example, Bokaie et al. [23] and Weng et al. [40] found 6 °C and 23.4 °C differences between IS and GS, which was much higher than this study. The difference in mean LST is primarily affected by landscape pattern, composition, topography, and satellite data [32]. It can be stated that landscape composition is the dominant factor affecting variation LST between IS, GS, and BS. For example, it was found that the percentage of GS and BS coverage was 0% at the buffer of 300 m, 100%, 96%, and 90% at the buffer 300 m, 600 m, and 900 m buffer zones. On the other hand, the percentage of GS and BS covers about 50% of the land use type at the buffer zone of 4500 m, and IS was 9%. Thus, landscape patterns significantly impacted the LST difference between IS, GS, and BS. LST had a significant positive correlation with IS and a significant negative correlation with GS and BS. These findings were similar to previous studies [32,37,40].

The GS and BS were larger and aggregated at the buffer zones located in fringe areas. This is the reason the urban core areas were characterized by the higher LST (due to higher aggregation of IS) in comparison to the fringe areas (due to higher aggregation of GS and BS) [32]. Three spatial metrics had a significant correlation with LST (positive correlation with IS and negative correlation with GS and BS). Similar findings were also reported in previous studies. For example, Li et al. [41] conducted a study in Beijing (China) and found a negative correlation between LST and the size and shape of GS. Zhou et al. [42] also showed a positive correlation between the size and shape of IS patches and a negative correlation with GS. Thus, the variation of LST is largely influenced by the edge characteristics of IS, GS, and BS patches [32,43]. The aggregation of IS, GS, and BS had a significantly strong correlation with the mean LST (strong positive with IS and strong negative with GS and BS) (Table 4). It denoted that those larger and contiguous patches of GS and BS had a stronger cooling impact than the smaller ones [41,44]. On the other hand, larger and contiguous patches of IS produce a stronger UHI effect than the smaller patches of IS [32].

Among three landscape metrics, AI showed a consistently significant correlation with IS, GS, and BS (positive with IS, negative with GS and BS). The aggregation of GS and BS generates a stronger cooling effect than the IS [32]. The results showed that higher aggregation of IS was characterized by high LST and a stronger UHI effect [32].

4.1. Policy Implications

The process of urbanization cannot be stopped or curtailed; it has been increasing over the periods. Well-planned measures and strategies can mitigate the consequences of rapid urban expansion and their impact on environmental problems. The cities as complex systems are largely determined by the various socio-economic factors [45]. The intensity of the construction lands increases with increasing urban human activities. Thus, IS intensifies the UHI effect and challenges sustainable development greatly [46]. The areas with high UHI intensity are mainly concentrated in the main urban areas, and core areas of the city are characterized by low GI. The UHI effect expanded outwards due to urban edge expansions [27]. The urban expansion in EBUA is affected by the large patches of impervious surface, green and blue patches. All these patches have a significant role in intensifying the UHI effect [47]. Thus, it is essential to understand the city's sustainable development and alleviate the UHI effect. The core areas of EBUA have overloaded due to filling urban expansion [27]. Thus, from the perspective of urban expansion, the local government (municipalities) must restrict unplanned construction. Secondly, the

UHI effect can also be mitigated through urban ecological perspectives. For example, an increase in GS and water areas must be promoted, and it can be integrated into the decision-making framework. Thirdly, mango orchards have a cooling effect in the Wetland (Chatra Wetland) [48]. The presence of the water bodies and GS not only improves the quality of life of the urban residents but also effectively alleviates the UHI effect.

In developing countries, rapid and unplanned urbanization has brought a series of environmental threats, such as the emergence of the UHI effect [7,49], loss of ecosystem services [50], and degradation of ecosystem health [51]. Therefore, it is an urgent task for scientists and engineers to overcome the UHI effect through proper planning and adaptation strategies. There are many techniques and tools to tackle the adverse effects of UHI, such as green roofs, cool pavements, urban geometry, and design (such as orientations, shape, and size) [52–54]. In addition, adopting and implementing urban gardens and green roads are significant cooling enhancers to reduce high temperatures in urban areas [55,56]. The urban and BSs in urban areas have a significant cooling effect [44,57]. Therefore, it is necessary to implement effective policies to protect and conserve green and BSs in urban areas.

Implementing innovative techniques to mitigate the UHI effect is a great challenge for developing countries (such as India). Therefore, emphasis must be given to the urban greening strategies to mitigate the UHI effect. Urban greening is a strategy through which urban GS are developed, maintained, and improved [32]. In addition, fragmented patches of GS and BS are less effective in mitigating the UHI effect than GS and BS clusters. Aggregating IS in an area dramatically increases temperature and promotes the UHI effect. Therefore, the spatial arrangements of urban landscapes need to be considered in the decision-making framework. The protection and conservation of GS and BS are not only important to mitigate the UHI effect but rather to achieve sustainable development goals (SDGs) such as Good Health and Well-Being (Goal 3), Sustainable Cities and Society (Goal 11), Climate Actions (Goal 13), and finally Life on Land (Goal 15).

4.2. Limitations and Future Research Directions

The study revealed significant landscape planning and management findings to mitigate the UHI effect. Still, this study has a few flaws. First, the impact of URG landscape composition and configuration was assessed for 2021, not for 2001 and 2011 (Figures 6 and 7). Therefore, in future studies, the urban–rural gradient can be assessed each year for a better understanding of the correlation of LST with IS, GS, and BS. Second, the 300 m buffer zones have been developed for the analysis of URG from the core of the city. Thus, micro-level analysis (such as a 100 m buffer zone) could be developed for better analysis. Thirdly, three spatial metrics have been used to understand the impact of landscape patterns on the LST to represent size, shape, and aggregation. More spatial metrics at the class and landscape level can be considered in future studies. Despite this limitation, this study provides significant insights into the spatial planning of the urban landscape to mitigate the UHI effect.

5. Conclusions

This study aims to understand the dynamics of land use, landscape composition, and configuration and their impact on the LST using Landsat 5 TM and OLI in an urban agglomeration in Eastern India. The spatial composition and configuration of impervious surfaces, GS, and BS have been examined from multiple geospatial and statistical perspectives (e.g., gradient approach and spatial metrics). From the results, a few notable research findings can be highlighted. There was a significant decrease in LST from the city's core towards fringe areas. LST declined by about 0.45 °C per kilometer from the core of the city. The areas with high and very high LSTVI increased in the last 20 years. The proportion of IS decreased, and GS and BS increased with increasing distance from the core area in EBUA. LST had a significant positive correlation with IS and a negative correlation with GS and BS. The size, shape, and aggregation of the landscape had a significant impact on the thermal

environment. Notably, the aggregation of IS had a consistent positive effect on LST. This suggests and highlights the importance of GS and BS, indicating that GS and BS need to be managed and persevered through effective planning strategies to mitigate climate change even in small and medium-sized cities. The planners and policymakers must focus on the core areas as these areas were characterized by high LST with a lower proportion of GS and BS.

Overall, this study provides evidence of the impact of landscape composition and configuration on the thermal environment in medium-sized urban agglomerations in developing countries. The mean LST of IS was higher than the GS and BS, indicating the importance of GS and BS in mitigating the UHI effect in cities. Therefore, it is essential to consider the spatial pattern of GS and BS in urban landscape and land use planning.

Supplementary Materials: The following supporting information can be downloaded at: https://www.mdpi.com/article/10.3390/su16031147/s1. Figure S1: Verificaiton of results from different location of the study area. Figure S2: LST map in EBUA (A) 2001 (B) 2011 and (C) 2021 (Buffer shows the distance with an interval of 300 m). Figure S3: Scatter plots showing the relationship between LST and impervious surface (A) 2001 (B) 2011 (C) 2021. Figure S4: Variation of landscape metrics along urban-rural gradient (A) area mean (B) shape mean and (C) aggregation index. Figure S5: Scatter plots showing the relationship between LST and spatial metrics. Impervious surface (A,D,G), green space (B,E,H) and blue space (C,F,I). Brown color indicates 'impervious surface', green color indicates 'green space' and blue color indicates 'blue space'.

Author Contributions: Conceptualization, M.D. and A.D.; methodology, M.D., A.D. and P.S.; software, M.D. and P.S.; validation, M.D. and A.D.; formal analysis, M.D. and A.D., investigation, M.D.; writing—original draft preparation, M.D., A.D. and R.D.; writing—review and editing, A.D., R.D., P.P. and M.I.; visualization, M.D.; supervision, A.D., R.D., P.P. and M.I. All authors have read and agreed to the published version of the manuscript.

Funding: This research received no external funding.

Institutional Review Board Statement: Not applicable.

Informed Consent Statement: Not applicable.

Data Availability Statement: The data used in this study are available on request from the corresponding author.

Conflicts of Interest: The authors declare no conflicts of interest.

References

1. Gallo, K.P.; Owen, T.W. Satellite-Based Adjustments for the Urban Heat Island Temperature Bias. *J. Appl. Meteorol.* **1999**, *38*, 806–813. [CrossRef]
2. Guo, G.; Wu, Z.; Xiao, R.; Chen, Y.; Liu, X.; Zhang, X. Impacts of urban biophysical composition on land surface temperature in urban heat island clusters. *Landsc. Urban Plan.* **2015**, *135*, 1–10. [CrossRef]
3. Lo, C.P.; Quattrochi, D.A.; Luvall, J.C. Application of high-resolution thermal infrared remote sensing and GIS to assess the urban heat island effect. *Int. J. Remote Sens.* **1997**, *18*, 287–304. [CrossRef]
4. Singh, P.; Kikon, N.; Verma, P. Impact of land use change and urbanisation on urban heat island in Lucknow city, Central India. A remote sensing based estimate. *Sustain. Cities Soc.* **2017**, *32*, 100–114. [CrossRef]
5. Du, H.; Ai, J.; Cai, Y.; Jiang, H.; Liu, P. Combined Effects of the Surface Urban Heat Island with Landscape Composition and Configuration Based on Remote Sensing: A Case Study of Shanghai, China. *Sustainability* **2019**, *11*, 2890. [CrossRef]
6. Soydan, O. Effects of landscape composition and patterns on land surface temperature: Urban heat island case study for Nigde, Turkey. *Urban Clim.* **2020**, *34*, 100688. [CrossRef]
7. Das, M.; Das, A. Exploring the pattern of outdoor thermal comfort (OTC) in a tropical planning region of eastern India during summer. *Urban Clim.* **2020**, *34*, 100708. [CrossRef]
8. Saha, S.; Saha, A.; Das, M.; Saha, A.; Sarkar, R.; Das, A. Analyzing spatial relationship between land use/land cover (LULC) and land surface temperature (LST) of three urban agglomerations (UAs) of Eastern India. *Remote Sens. Appl. Soc. Environ.* **2021**, *22*, 100507. [CrossRef]
9. Kedia, S.; Bhakare, S.P.; Dwivedi, A.K.; Islam, S.; Kaginalkar, A. Estimates of change in surface meteorology and urban heat island over northwest India: Impact of urbanisation. *Urban Clim.* **2021**, *36*, 100782. [CrossRef]

10. Howard, L. The Climate of London: Deduced from Meteorological Observations Made in the Metropolis and at Various Places Around It. 1833, Volume 3. Available online: https://wellcomecollection.org/works/y73fcwsn (accessed on 29 December 2023).
11. Voogt, J.A. *Urban Heat Islands: Hotter Cities*; America Institute of Biological Sciences: Herndon, VA, USA, 2004.
12. Zhang, M.; Dong, S.; Cheng, H.; Li, F. Spatio-temporal evolution of urban thermal environment and its driving factors: Case study of Nanjing, China. *PLoS ONE* **2021**, *16*, e0246011. [CrossRef]
13. Coseo, P.; Larsen, L. How factors of land use/land cover, building configuration, and adjacent heat sources and sinks explain Urban Heat Islands in Chicago. *Landsc. Urban Plan.* **2014**, *125*, 117–129. [CrossRef]
14. Debbage, N.; Shepherd, J.M. The urban heat island effect and city contiguity. *Comput. Environ. Urban Syst.* **2015**, *54*, 181–194. [CrossRef]
15. Lin, J.; Wei, K.; Guan, Z. Exploring the connection between morphological characteristic of built-up areas and surface heat islands based on MSPA. *Urban Clim.* **2024**, *53*, 101764. [CrossRef]
16. Huang, Q.; Lu, Y. Urban heat island research from 1991 to 2015: A bibliometric analysis. *Theor. Appl. Clim.* **2018**, *131*, 1055–1067. [CrossRef]
17. Deng, Y.; Wang, S.; Bai, X.; Tian, Y.; Wu, L.; Xiao, J.; Chen, F.; Qian, Q. Relationship among land surface temperature and LUCC, NDVI in typical karst area. *Sci. Rep.* **2018**, *8*, 64. [CrossRef] [PubMed]
18. Guha, S.; Govil, H.; Dey, A.; Gill, N. Analytical study of land surface temperature with NDVI and NDBI using Landsat 8 OLI and TIRS data in Florence and Naples city, Italy. *Eur. J. Remote Sens.* **2018**, *51*, 667–678. [CrossRef]
19. Maimaitiyiming, M.; Ghulam, A.; Tiyip, T.; Pla, F.; Latorre-Carmona, P.; Halik, Ü.; Sawut, M.; Caetano, M. Effects of green space spatial pattern on land surface temperature: Implications for sustainable urban planning and climate change adaptation. *ISPRS J. Photogramm. Remote Sens.* **2014**, *89*, 59–66. [CrossRef]
20. Asgarian, A.; Amiri, B.J.; Sakieh, Y. Assessing the effect of green cover spatial patterns on urban land surface temperature using landscape metrics approach. *Urban Ecosyst.* **2015**, *18*, 209–222. [CrossRef]
21. Sun, R.; Chen, L. Effects of green space dynamics on urban heat islands: Mitigation and diversification. *Ecosyst. Serv.* **2017**, *23*, 38–46. [CrossRef]
22. Zhang, H.; Qi, Z.-F.; Ye, X.-Y.; Cai, Y.-B.; Ma, W.-C.; Chen, M.-N. Analysis of land use/land cover change, population shift, and their effects on spatiotemporal patterns of urban heat islands in metropolitan Shanghai, China. *Appl. Geogr.* **2013**, *44*, 121–133. [CrossRef]
23. Bokaie, M.; Zarkesh, M.K.; Arasteh, P.D.; Hosseini, A. Assessment of Urban Heat Island based on the relationship between land surface temperature and Land Use/ Land Cover in Tehran. *Sustain. Cities Soc.* **2016**, *23*, 94–104. [CrossRef]
24. Irfeey, A.M.M.; Chau, H.-W.; Sumaiya, M.M.F.; Wai, C.Y.; Muttil, N.; Jamei, E. Sustainable Mitigation Strategies for Urban Heat Island Effects in Urban Areas. *Sustainability* **2023**, *15*, 10767. [CrossRef]
25. Shukla, A.; Jain, K. Critical analysis of rural-urban transitions and transformations in Lucknow city, India. *Remote Sens. Appl. Soc. Environ.* **2019**, *13*, 445–456. [CrossRef]
26. Grover, A.; Singh, R.B. Analysis of urban heat island (UHI) in relation to normalised difference vegetation index (NDVI): A comparative study of Delhi and Mumbai. *Environments* **2015**, *2*, 125–138. [CrossRef]
27. Dutta, I.; Das, A. Exploring the dynamics of urban sprawl using geo-spatial indices: A study of English Bazar Urban Agglomeration, West Bengal. *Appl. Geomat.* **2019**, *11*, 259–276. [CrossRef]
28. Pal, S.; Ziaul, S. Detection of land use and land cover change and land surface temperature in English Bazar urban centre. *Egypt. J. Remote Sens. Space Sci.* **2017**, *20*, 125–145.
29. Dutta, I.; Das, A. Exploring the Spatio-temporal pattern of regional heat island (RHI) in an urban agglomeration of secondary cities in Eastern India. *Urban Clim.* **2020**, *34*, 100679. [CrossRef]
30. Ziaul, S.; Pal, S. Assessing outdoor thermal comfort of English Bazar Municipality and its surrounding, West Bengal, India. *Adv. Space Res.* **2019**, *64*, 567–580. [CrossRef]
31. Kikon, N.; Singh, P.; Singh, S.K.; Vyas, A. Assessment of urban heat islands (UHI) of Noida City, India using multi-temporal satellite data. *Sustain. Cities Soc.* **2016**, *22*, 19–28. [CrossRef]
32. Estoque, R.C.; Murayama, Y.; Myint, S.W. Effects of landscape composition and pattern on land surface temperature: An urban heat island study in the megacities of Southeast Asia. *Sci. Total Environ.* **2017**, *577*, 349–359. [CrossRef]
33. Liu, G.; Zhang, Q.; Li, G.; Doronzo, D.M. Response of land cover types to land surface temperature derived from Landsat-5 TM in Nanjing Metropolitan Region, China. *Environ. Earth Sci.* **2016**, *75*, 1386. [CrossRef]
34. McGarigal, K.; Cushman, S.A.; Neel, M.C.; Ene, E. FRAGSTATS: Spatial Pattern Analysis Program for Categorical Maps. Computer Software Program Produced by the Authors at the University of Massachusetts, Amherst. 2002. Available online: https://www.umass.edu/landeco/research/fragstats/fragstats.html (accessed on 29 December 2023).
35. Boori, M.S.; Choudhary, K.; Paringer, R.; Kupriyanov, A. Spatiotemporal ecological vulnerability analysis with statistical correlation based on satellite remote sensing in Samara, Russia. *J. Environ. Manag.* **2021**, *285*, 112138. [CrossRef] [PubMed]
36. Luo, J.; Zhuo, W.; Liu, S.; Xu, B. The Optimization of Carbon Emission Prediction in Low Carbon Energy Economy under Big Data. *IEEE Access* **2024**. [CrossRef]
37. Myint, S.W.; Brazel, A.; Okin, G.; Buyantuyev, A. Combined effects of impervious surface and vegetation cover on air temperature variations in a rapidly expanding desert city. *GIScienceRemote Sens.* **2010**, *47*, 301–320. [CrossRef]

38. Sun, Q.; Wu, Z.; Tan, J. The relationship between land surface temperature and land use/land cover in Guangzhou, China. *Environ. Earth Sci.* **2012**, *65*, 1687–1694. [CrossRef]
39. Song, J.; Du, S.; Feng, X.; Guo, L. The relationships between landscape compositions and land surface temperature: Quantifying their resolution sensitivity with spatial regression models. *Landsc. Urban Plan.* **2014**, *123*, 145–157. [CrossRef]
40. Shang, K.; Xu, L.; Liu, X.; Yin, Z.; Liu, Z.; Li, X.; Yin, L.; Zheng, W. Study of Urban Heat Island Effect in Hangzhou Metropolitan Area Based on SW-TES Algorithm and Image Dichotomous Model. *SAGE Open* **2023**, *13*. [CrossRef]
41. Li, X.; Zhou, W.; Ouyang, Z.; Xu, W.; Zheng, H. Spatial pattern of greenspace affects land surface temperature: Evidence from the heavily urbanised Beijing metropolitan area, China. *Landsc. Ecol.* **2012**, *27*, 887–898. [CrossRef]
42. Zhou, W.; Huang, G.; Cadenasso, M.L. Does spatial configuration matter? Understanding the effects of land cover pattern on land surface temperature in urban landscapes. *Landsc. Urban Plan.* **2011**, *102*, 54–63. [CrossRef]
43. Connors, J.P.; Galletti, C.S.; Chow, W.T.L. Landscape configuration and urban heat island effects: Assessing the relationship between landscape characteristics and land surface temperature in Phoenix, Arizona. *Landsc. Ecol.* **2013**, *28*, 271–283. [CrossRef]
44. Das, M.; Das, A.; Momin, S. Quantifying the cooling effect of urban green space: A case from urban parks in a tropical mega metropolitan area (India). *Sustain. Cities Soc.* **2022**, *87*, 104062. [CrossRef]
45. Wang, R.; Li, F.; Hu, D.; Li, B.L. Understanding eco-complexity: Social-Economic-Natural Complex Ecosystem approach. *Ecol. Complex.* **2011**, *8*, 15–29. [CrossRef]
46. Shen, H.; Huang, L.; Zhang, L.; Wu, P.; Zeng, C. Long-term and fine-scale satellite monitoring of the urban heat island effect by the fusion of multi-temporal and multi-sensor remote sensed data: A 26-year case study of the city of Wuhan in China. *Remote Sens. Environ.* **2016**, *172*, 109–125. [CrossRef]
47. Tian, P.; Li, J.; Cao, L.; Pu, R.; Wang, Z.; Zhang, H.; Chen, H.; Gong, H. Assessing spatiotemporal characteristics of urban heat islands from the perspective of an urban expansion and green infrastructure. *Sustain. Cities Soc.* **2021**, *74*, 103208. [CrossRef]
48. Yang, H.; Zhang, X.; Li, Z.; Cui, J. Region-Level Traffic Prediction Based on Temporal Multi-Spatial Dependence Graph Convolutional Network from GPS Data. *Remote Sens.* **2022**, *14*, 303. [CrossRef]
49. Zhou, X.; Chen, H. Impact of urbanisation-related land use land cover changes and urban morphology changes on the urban heat island phenomenon. *Sci. Total Environ.* **2018**, *635*, 1467–1476. [CrossRef]
50. Das, M.; Das, A. Dynamics of Urbanization and its impact on Urban Ecosystem Services (UESs): A study of a medium size town of West Bengal, Eastern India. *J. Urban Manag.* **2019**, *8*, 420–434. [CrossRef]
51. Das, M.; Das, A.; Pereira, P.; Mandal, A. Exploring the spatio-temporal dynamics of ecosystem health: A study on a rapidly urbanising metropolitan area of Lower Gangetic Plain, India. *Ecol. Indic.* **2021**, *125*, 107584. [CrossRef]
52. Qin, Y. A review on the development of cool pavements to mitigate urban heat island effect. *Renew. Sustain. Energy Rev.* **2015**, *52*, 445–459. [CrossRef]
53. Lu, S.; Zhu, G.; Meng, G.; Lin, X.; Liu, Y.; Qiu, D.; Xu, Y.; Wang, Q.; Chen, L.; Li, R.; et al. Influence of atmospheric circulation on the stable isotope of precipitation in the monsoon margin region. *Atmos. Res.* **2024**, *298*, 107131. [CrossRef]
54. Sharma, A.; Conry, P.; Fernando, H.J.S.; Hamlet, A.F.; Hellmann, J.J.; Chen, F. Green and cool roofs to mitigate urban heat island effects in the Chicago metropolitan area: Evaluation with a regional climate model. *Environ. Res. Lett.* **2016**, *11*, 064004. [CrossRef]
55. Saaroni, H.; Amorim, J.H.; Hiemstra, J.A.; Pearlmutter, D. Urban Green Infrastructure as a tool for urban heat mitigation: Survey of research methodologies and findings across different climatic regions. *Urban Clim.* **2018**, *24*, 94–110. [CrossRef]
56. Farhadi, H.; Faizi, M.; Sanaieian, H. Mitigating the urban heat island in a residential area in Tehran: Investigating the role of vegetation, materials, and orientation of buildings. *Sustain. Cities Soc.* **2019**, *46*, 101448. [CrossRef]
57. Aram, F.; Solgi, E.; García, E.H.; Mosavi, A.; Várkonyi-Kóczy, A.R. The Cooling Effect of Large-Scale Urban Parks on Surrounding Area Thermal Comfort. *Energies* **2019**, *12*, 3904. [CrossRef]

Disclaimer/Publisher's Note: The statements, opinions and data contained in all publications are solely those of the individual author(s) and contributor(s) and not of MDPI and/or the editor(s). MDPI and/or the editor(s) disclaim responsibility for any injury to people or property resulting from any ideas, methods, instructions or products referred to in the content.